A NON-DIMENSIONAL SURROGATE MODEL OF STRATIFIED FILLING DURING INDOOR, PLUME-LIKE HYDROGEN RELEASES

Vanlaere, J.[1,2,*], Hendrick, P.[1] and Blondeau, J.[2]

[1] Aero-Thermo-Mechanics Laboratory, Université Libre de Bruxelles (ULB), Avenue F.D. Roosevelt, 50 (CP 165/41), Brussels, 1050, Belgium, joren.vanlaere@ulb.be
[2] Thermo and Fluid Dynamics (FLOW), Faculty of Engineering, Vrije Universiteit Brussel (VUB), Pleinlaan, 2, Brussels, 1050, Belgium

ABSTRACT

Hydrogen is commonly used as feedstock in industrial processes and is regarded as a potential future energy carrier. However, its reactivity and low density make it difficult to handle and store safely. Indoor hydrogen dispersion can cause a fire or explosion hazard if encountering an ignition source. Safety practices often use time expensive modelling techniques to estimate risk associated with hydrogen. A neural network based surrogate model could efficiently replace Computational Fluid Dynamics (CFD) modelling in safety studies. To lower the dimensionality of this surrogate model, a dimensional analysis based on Buckingham's Pi-theorem is proposed. The dimensional analysis examines stratified filling and highlights the functional parameters involved in the process. Stratified filling occurs for buoyancy dominated releases and is characterized by layers of decreasing concentration starting at the ceiling of the enclosure and developing towards the bottom. The study involves four dimensional cases that were simulated using Computational Fluid Dynamics (CFD) to demonstrate the usefulness of the proposed dimensionless time and dimensionless volume. The setup considered in this paper consists of a parallelepiped enclosure with standard atmospheric conditions, a single release source and one pressure outlet to ensure constant pressure during the release. The results of the CFD simulations show a distinct pattern in the relation of hydrogen molar fraction and dimensionless time. The pattern depends on the dimensionless height of the measurement location. A five-parameter logistic (5PL) function is proposed to fit the data from the CFD models. Overall, the paper provides insights into the functional parameters involved in the evolution of hydrogen mass fractions during stratified filling. It provides a non-dimensional surrogate model to compute the evolution of the local concentrations of hydrogen during the development of stratification layers.

NOMENCLATURE

d	–	diameter
E	–	energy
F	–	force
g	–	gravitational constant
H	–	distance release source to ceiling
h	–	height
h^*	–	dimensionless height
l	–	number of dimensionless groups
J	–	diffusion flux
k_{eff}	–	effective conductivity
m	–	number of dimensions
n	–	number of functional parameters
p	–	pressure
Q	–	functional parameter
r	–	radius
R	–	net production rate
r^*	–	dimensionless radius
S	–	rate of creation

t	–	time
t^*	–	dimensionless time
V	–	total volume of the enclosure
v	–	velocity
$\dot{V}$	–	volumetric flow rate
w	–	width
x	–	x-coordinate
Y	–	mass fraction
y	–	y-coordinate
z	–	z-coordinate
Π	–	dimensionless group
τ	–	stress tensor
ρ	–	density
χ_j	–	molar fraction of species j

Subscripts

a	–	air
d	–	measurement location
gc	–	gravity current
h_2	–	hydrogen
p	–	plume
t	–	overturning
0	–	release source

1. INTRODUCTION

Hydrogen is commonly used as feedstock in various industrial processes and a potential future energy carrier. However, its reactivity and low density make it challenging to handle and store safely. In the event of a hydrogen release, the gas disperses rapidly creating a potential fire or explosion hazard if it encounters an ignition source. Therefore, indoor hydrogen dispersion is a significant safety concern for various applications including technical rooms, residential garages [1], workshops, and nuclear reactors [2]. A surrogate model representing time series of hydrogen mass fraction could improve safety engineering practices. This model can be used to optimize detector layout in closed spaces and determine the development of flammable volumes during a release. With the underlying aim of building such a model, this paper discusses stratified filling during plume-like hydrogen releases in semi-closed spaces. Previous experimental [1], [3], [4] and numerical studies [5], [6] have investigated indoor hydrogen releases in parallelepiped or cylindrical enclosures. A common temporal pattern is observed, which can be described by two main parameters: the instant at which the hydrogen concentration rises and the rate at which the concentration rises. Based on these studies, it is expected that a limited number of functional parameters determine this pattern. The number of variables have a large impact on the number of required samples to train a surrogate model. A dimensional analysis, leading to the use of relevant non-dimensional parameters, can lower the number of variables, and reduce the impact of the curse of dimensionality [7]. In this paper a dimensional analysis, based on Buckingham's Pi-theorem, is proposed to examine stratified filling and highlight the functional parameters involved in the process. The study involves four dimensional cases, that were simulated using Computational Fluid Dynamics (CFD), to demonstrate the usefulness of the proposed dimensionless time and dimensionless volume. Volumetric flow rate and total volume is varied across the models to examine the effects on molar fraction and time. The setup considered in this paper consists of a parallelepiped enclosure with standard atmospheric conditions. Pure hydrogen is released from a single release source. A ventilation hole in the floor is modelled to maintain atmospheric pressure in the room during the release. The outline of the paper is as follows: Firstly, the macroscopic features of plume-like releases of buoyant gases are explained. Following, a dimensional analysis is performed to describe the evolution of hydrogen mass fraction during the filling regime. Section 4 presents the properties of the CFD models that are used to

validate the dimensional analysis. Finally, the results of the CFD models are compared with the dimensional analysis and discussed.

2. BACKGROUND

In this section, the main features of plume-like releases of buoyant gases in semi-closed spaces are discussed. Fig. 1 visualizes a schematic representation of the situation. At first, an upward plume is formed from the orifice (Fig. 1, red). As the plume collides with the ceiling, the buoyant gas starts spreading outwards from the plume's axis (Fig. 1, green). This flow is called a gravity current and due to buoyancy it happens close to the ceiling [8]. This outward movement is stopped by the walls, forcing the gas to a downward motion called overturning (Fig. 1, yellow). All this happens during the initial phase of the release. In the second phase, the gas starts filling the room from the ceiling down.

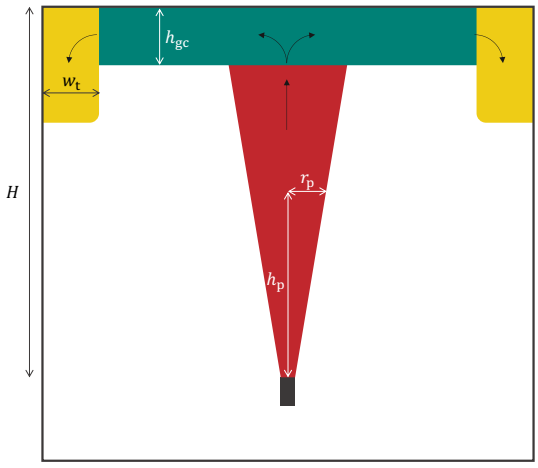

Figure 1. Schematic representation of an indoor, plume-like release of a buoyant gas. Adapted from [9].

There has been extensive research about buoyant plume dynamics. Morton [8] provides a mathematical formulation for the distribution of flow rate, momentum, and buoyancy fluxes in plumes. The conical shape of the plume is a result of mixing with the surrounding air, thus increasing volumetric flow rate and radius. Based on this research, Kaye and Hunt [10] further developed these mathematical relations. The radius r_p of the plume follows a linear relation with height h_p from the orifice and entrainment coefficient α [10]. The entrainment coefficient is constant for a given case but depends on the momentum at the orifice.
A distinction is made between forced plumes, as studied in [8] and [10] and lazy plumes as introduced in another paper by Kaye and Hunt [11]. The gravity current and overturning has been discussed in [10] and [9]. Kaye and Hunt [10], experimentally determined a relation for thickness h_c of the developed gravity current. h_c is a function of distance H. Following relation was published: $h_c = 0.12 \cdot H$, or approximately $H/8$. Overturning was also discussed in [10]. The width of the overturning, w_t, depends on the aspect ratio of the enclosure [10]. For small aspect ratios, it happens in the region with distance H from the wall. For large aspect ratios, the phenomenon reaches up to the plume's axis. However, the assumption made in [10] is that the release is in the middle of the enclosure. In this study, the release location is variable throughout the complete domain. Thus, the development of the gravity current is also function of the location of the release source, relative to the wall.
After the gravity current reaches the wall, the room starts filling with buoyant gas. Kaye and Hunt [10] introduced the filling box model. The main feature of this model is the stratification process where the room fills with layers of decreasing concentration. [12] and [13] discussed momentum dominated releases where more mixing is present. The result is a less pronounced stratification layer compared to the filling box model. Denisenko [14] calls this second model the fading up model. The volume Richardson number is used by [13]-[15] to define the filling regime based on the release characteristics. Overall, previous research provides detailed information on plume-like releases of buoyant gases.

However, the relations developed in these studies have complex formulations. These formulations give a good insight into the physics, but their formulations make them hard to understand and apply. In the following section, simple relations between the functional parameters are proposed using under the form of a non-dimensional surrogate model generated from CFD simulations, using Buckingham's Pi-theorem. Based on CFD simulations, the complexity of the relation is visualized in Section 5.

3. DIMENSIONAL ANALYSIS

To develop simple relations between the functional parameters of stratified filling in a semi-closed space, a dimensional analysis is performed. Buckingham's Pi-theorem is an ideal candidate for this purpose. [16] states that: Suppose that a physical problem can be described using the following equation:

$$f(\mathrm{Q}_1, \mathrm{Q}_2, \ldots, \mathrm{Q}_n) = 0, \tag{1}$$

where Q_i are the functional parameters of the problem. if the n parameters Q_i contain m primary dimensions, then $l\ (n-m)$ dimensionless groups can be constructed, such that the following relation holds between these dimensionless groups:

$$\psi(\Pi_1, \Pi_2, \ldots, \Pi_l) = 0, \tag{2}$$

Each dimensionless group Π_i is function of the original parameters.

$$\Pi_i = Q_1^{\mathrm{k}_1} \cdot Q_2^{\mathrm{k}_2} \cdot \ldots \cdot Q_n^{\mathrm{k}_n}, \tag{3}$$

In this study, a dimensionless analysis is developed for stratified filling of an enclosure during the release of a buoyant gas. Ten functional parameters are considered: Molar fraction of hydrogen $\left(\chi_{\mathrm{h}_2}\right)$, time (t), volumetric flow rate $\left(\dot{V}\right)$, height of the release source (h_0), height of the measurement location (h_d), length (l), width (w), and height (h) of the geometry, gas density (ρ_0), and air density (ρ_a). These functional parameters and their dimensions are summarized in Table 1.

Table 1. Proposed functional parameters of stratified filling with their units.

	χ_{h_2}	t	$\dot{V}$	h_0	h_d	l	w	h	ρ_0	ρ_a
[m]	0	0	3	1	1	1	1	1	-3	-3
[s]	0	1	1	0	0	0	0	0	0	0
[kg]	0	0	0	0	0	0	0	0	1	1

As a result, Equation (1) becomes:

$$f\left(\chi_{\mathrm{h}_2}, t, \dot{V}, h_0, h_\mathrm{d}, l, w, h, \rho_0, \rho_a\right) = 0, \tag{4}$$

Three (m) primary dimensions describe these ten (n) functional parameters; Hence, seven (l) dimensionless groups can be constructed. Therefore, seven (l) fundamental parameter must be chosen; χ_{h_2}, t, h_0, h_d, l, w, and ρ_0 are used in this paper. The other three $(n-l)$ quantities are regarded as derived parameters. They are $\dot{V}$, h, and ρ_a.

The dimensionless groups become,

$$\Pi_1 = \dot{V}^0 \cdot h^0 \cdot {\rho_\mathrm{a}}^0 \cdot \chi_{h_2} = \chi_{h_2}, \tag{5}$$

$$\Pi_2 = \dot{V}^1 \cdot h^{-3} \cdot {\rho_\mathrm{a}}^0 \cdot t = \frac{\dot{V} \cdot t}{h^3}, \tag{6}$$

$$\Pi_3 = \dot{V}^0 \cdot h^{-1} \cdot {\rho_\mathrm{a}}^0 \cdot h_0 = \frac{h_0}{h}, \tag{7}$$

$$\Pi_4 = \dot{V}^0 \cdot h^{-1} \cdot {\rho_a}^0 \cdot h_d = \frac{h_d}{h}, \quad (8)$$

$$\Pi_5 = \dot{V}^0 \cdot h^{-1} \cdot {\rho_a}^0 \cdot l = \frac{l}{h}, \quad (9)$$

$$\Pi_6 = \dot{V}^0 \cdot h^{-1} \cdot {\rho_a}^0 \cdot w = \frac{w}{h}, \quad (10)$$

$$\Pi_7 = \dot{V}^0 \cdot h^0 \cdot {\rho_a}^{-1} \cdot \rho_0 = \frac{\rho_0}{\rho_a}, \quad (11)$$

Consequently, Equation (2) leads to Equation (12).

$$\psi\left(\chi_{H_2}, \frac{\dot{V} \cdot t}{h^3}, \frac{h_d}{h}, \frac{h_0}{h}, \frac{l}{h}, \frac{w}{h}, \frac{\rho_0}{\rho_a}\right) = 0, \quad (12)$$

For readability, following dimensionless parameters are defined. Firstly, the dimensionless height of the measurement location:

$${h_d}^* = \frac{h_d}{h}, \quad (13)$$

where h_d – vertical distance from the floor to the measurement location, m; h – height of the enclosure, m. Secondly, the dimensionless height of the orifice:

$${h_0}^* = \frac{h_0}{h}, \quad (14)$$

where h_0 – vertical distance from the floor to the orifice, m; h – height of the enclosure, m. Lastly, dimensionless time is defined:

$$t^* = \frac{\dot{V} \cdot t}{V}, \quad (15)$$

Where V is the total volume of the enclosure. If l/h and w/h are constant, V is proportional to h^3. As a result, t^* is equivalent to $\frac{\dot{V} \cdot t}{h^3}$. Based on these definitions, Equation (12) becomes:

$$\psi\left(\chi_{H_2}, t^*, {h_d}^*, {h_0}^*, \frac{l}{W}, \frac{l}{h}, \frac{\rho_0}{\rho_a}\right) = 0, \quad (16)$$

This dimensional analysis is further used in Section 5 to derive a non-dimensional surrogate model able to predict the evolution of the concentration of hydrogen in the enclosure in filling regime. The model is based on the results of CFD simulations performed for four different, although similar, cases.

4. CFD MODEL

The four CFD simulations were performed using Ansys Fluent. This paper simplifies the problem and mainly focusses on the relation between χ_{H_2} and t^*. The number of dimensions can therefore be reduced as follows. All four cases have the same dimensionless coordinates $\left(\frac{x}{h}, \frac{y}{h}, \frac{z}{h}\right)$ of the release source $\left(\frac{1}{10}, \frac{-5}{10}, \frac{-4}{10}\right)$, $\frac{l}{h}$ (2), and $\frac{w}{h}$ (1). As a result, the value for the dimensional height of the release source (${h_0}^*$) becomes $\frac{1}{10}$. The values of $\dot{V}$ and V are sampled using Latin Hypercube Sampling. In this paper, the dimensions of the geometry are limited from lab scale to the scale of a small technical room. In future work, the dimensions of the geometry will be enlarged to cover industrial applications as well. The release source is located out of center and close to the ground plane as shown in Fig. 2. This set up limits the influence of symmetrical flow features caused by the release of hydrogen. The main parameters of the four cases can be consulted in Table 2. In this study, no experimental data is available for model validation. Fig. 2 (a) shows a schematic representation of the geometry. The circular orifice is defined

by its diameter d_0. The velocity at the orifice is fixed at 10 m/s and the volumetric flow rate is calculated with Equation (17); thus, varying d_0 controls the volumetric flow rate of the release.

$$\dot{V} = \pi \cdot \left({}^{d_0}/_{2}\right)^2, \tag{17}$$

where $\dot{V}$ – volumetric flow rate, m^3/s; d_0 – orifice diameter, m.

Table 2. Sampled values for volumetric flow rate $\dot{V}$ and total volume V using Latin Hypercube Sampling and the dimensionless groups that are fixed across all cases.

Case	$\dot{V}$ $[\mathrm{m}^3/s]$	V $[\mathrm{m}^3]$	${h_0}^*$	l/h	w/h	ρ_0/ρ_a
1	0.021	9.809	1/10	2	1	0.0899/1.225
2	0.061	3.195	1/10	2	1	0.0899/1.225
3	0.077	12.622	1/10	2	1	0.0899/1.225
4	0.034	4.737	1/10	2	1	0.0899/1.225

The evolution of hydrogen mass fraction is monitored in 152 locations at eight different values of ${h_d}^*$(ranging from 2/10 to 9/10 with intervals of 1/10), as illustrated in Fig 2 (b). Based on this data, it is possible to discuss the influence of ${h_d}^*$in equation (16). The geometry is designed with one opening at the bottom to ensure constant pressure in the enclosure. The radius of this opening is fixed at 50 mm. Additionally, a cylindrical release pod (200 mm by 100 mm) was modelled. Hydrogen releases from a circular orifice on top of this pod.

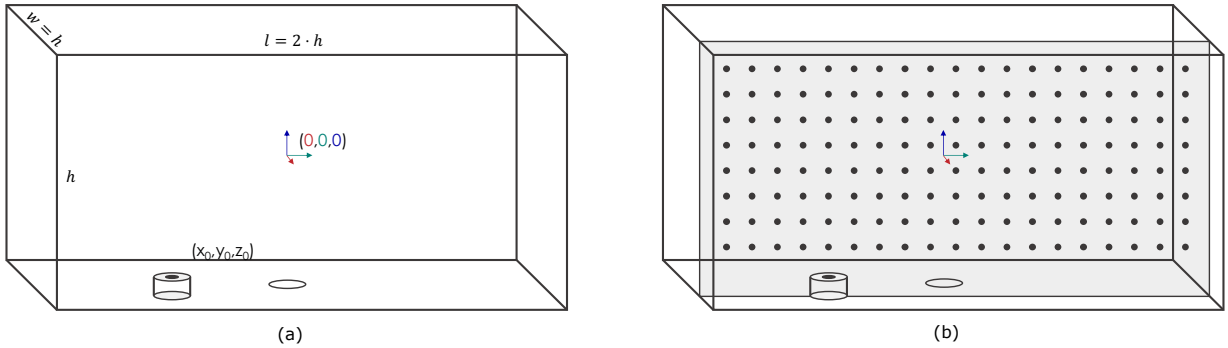

Figure 2. (a) Schematic representation of modelled geometry with release pod, orifice, and global coordinate system; (b) Grid of measurement locations, vertically oriented and normal to the orifice.

The meshing parameters used in this study are based on the guidelines from the SUSANA project [17]. A mesh with a base size of 60 mm is adopted. However, a finer mesh is employed close to the orifice. Six inflation layers with a total thickness of 5 mm ensured better accuracy near the wall. The accuracy of the wall treatment was evaluated using Y+ values.
The governing equations of the solver are the continuity equation, Navier-Stokes equation including gravitational forces, energy equation and species transport equation. The mass and momentum conservation equations are given by Equations (18) and (19):

$$\frac{\partial \rho}{\partial t} + \nabla \cdot (\rho \vec{v}) = 0, \tag{18}$$

where ρ – density, $\mathrm{kg/m}^3$; t – time, s; v – velocity, $\mathrm{m/s}$.

$$\frac{\partial (\rho \vec{v})}{\partial t} + \nabla \cdot (\rho \vec{v} \vec{v}) = -\nabla p + \nabla \bar{\bar{\tau}} + \rho \vec{g} + \vec{F}, \tag{19}$$

where ρ – density, $\mathrm{kg/m}^3$; v – velocity, $\mathrm{m/s}$; t – time, s; p – pressure, $\mathrm{kg/m \cdot s}^2$; $\bar{\bar{\tau}}$ – stress tensor, $\mathrm{kg/m \cdot s}^2$; $\vec{g}$ – gravitational constant, $\mathrm{m/s}^2$; $\vec{F}$, – external body force, $\mathrm{kg \cdot m}^2/\mathrm{s}^2$.

The energy equation, as solved by Ansys Fluent is presented in Equation (20) [18].

$$\frac{\partial(\rho E)}{\partial t} + \nabla \cdot \left(\vec{v}(\rho E + p)\right) = \nabla \cdot \left(k_{\text{eff}} \nabla T - \sum_{\text{j}} h_{\text{j}} \vec{J}_{\text{j}} + (\bar{\bar{\tau}}_{\text{eff}} \cdot \vec{v})\right) + S_{\text{h}}, \tag{20}$$

where ρ – density, kg/m^3; E – energy, $\text{kg} \cdot \text{m}^2/\text{s}^2$; t – time, s; v – velocity, m/s; p – pressure, $\text{kg/m} \cdot \text{s}^2$; k_{eff} – effective conductivity, $\text{kg} \cdot \text{m/s}^3 \cdot \text{K}$; T– temperature, K; h_{j} – specific enthalpy of species j, m^2/s^2; $\vec{J}_{\text{j}}$– diffusion flux of species j, $\text{kg/s} \cdot \text{m}^2$; $\bar{\bar{\tau}}$ – stress tensor, $\text{kg/m} \cdot \text{s}^2$; S_{h} – includes the heat of chemical reaction and any other volumetric heat sources that are defined. Finally, the species transport equation, given by Equation (21), predicts the local mass fraction of each species present in the flow [18].

$$\frac{\partial(\rho Y_{\text{j}})}{\partial t} + \nabla \cdot \left(\rho \vec{v} Y_{\text{j}}\right) = -\nabla \cdot \vec{J}_{\text{j}} + R_{\text{j}} + S_{\text{j}}, \tag{21}$$

Where ρ – density, kg/m^3; Y_{j} – mass fraction of species j, /; t – time, s; v – velocity, m/s; $\vec{J}_{\text{j}}$ –diffusion flux of species j, $\text{kg/s} \cdot \text{m}^2$; R_{j} – net production rate of species j by chemical reaction; S_{j} – rate of creation by addition from the dispersed phase plus any user-defined sources. To set up the solver, the guidelines proposed in the SUSANA project [17] are followed. In the enclosure, both turbulent, transitional, and laminar regions are expected. Most Reynolds-Averaged Navier-Stokes (RANS) models assume fully turbulent flow. Therefore, three-dimensional RANS equations with Renormalization group (RNG) $\kappa - \epsilon$ model for closure were chosen as it can reproduce turbulent, transitional, and laminar flow.

5. RESULTS & DISCUSSION

In this section, the results of the CFD simulations are discussed and used to derive a non-dimensional surrogate model, able to predict the evolution of hydrogen mass fractions in the enclosure during a stratified filling regime. Fig. 3a depicts the time series of hydrogen mass fractions for the four simulated cases, across all 152 measurement locations, up to 100 seconds after the release onset. Two trends can be observed. The first trend is a steady increase in molar fraction from 0 to 1. The second trend is an abrupt rise to a molar fraction between 0 and 1, followed by a slower increase towards the asymptote. The latter trend is a superposition of the sudden development of the plume and the slower development of the stratification layer and is therefore mainly observed in the plume. In this paper, the effects in the plume are not further discussed, and the focus is on the evolution of the hydrogen mass fractions during stratified filling, far from the plume. The measurement points in the plume are excluded in further results, based on a linear relation developed by [8] and [10]. Fig. 1 (Section 2) schematically shows this relation between r_{p} and h_{p}. A dimensionless radius $r_{\text{p}}{}^*$, based on these parameters, is presented in Equation (22), equivalent to the entrainment coefficient α defined by [8] and [10]. α is constant for a given plume according to [8] and [10] and is numerically defined using the vertical velocity profile near the plume. In non-dimensional terms, the plume is here roughly defined as that part of the domain where $r_{\text{d}}{}^*$ is less than $1/3$.

$$r_{\text{p}}{}^* = \frac{r_{\text{p}}}{h_{\text{p}}}. \tag{22}$$

Fig. 3b plots the dimensional time series at locations where $r_{\text{d}}{}^*$ is larger than $1/3$, i.e., far from the plume. It confirms that the second trend, described above, is related to the rapid development of the plume. It also shows that the dimensional patterns largely depend on the modelled case. In a first, (dimensional) approach, the ratio $\dot{V}/V$ is used to explain the differences between the four cases. Table 3 compares these ratios. It can be concluded that a larger ratio of $\dot{V}/V$ results in a steeper rise. Cases 3 and 4 have similar values for $\dot{V}/V$, and indeed show a similar pattern in their time series. A non-dimensional approach is used in Fig. 3c, where results far from the plume are plotted as a function of the dimensionless group t^* instead of time. All four models harmonize to a single pattern, illustrating the usefulness of a non-dimensional approach. As stated in Equation (12), the evolution of mass fractions

is also a function of relative height ${h_d}^*$. For the large values of ${r_d}^*$ considered here, it is expected that ${h_d}^*$ plays a less significant role.

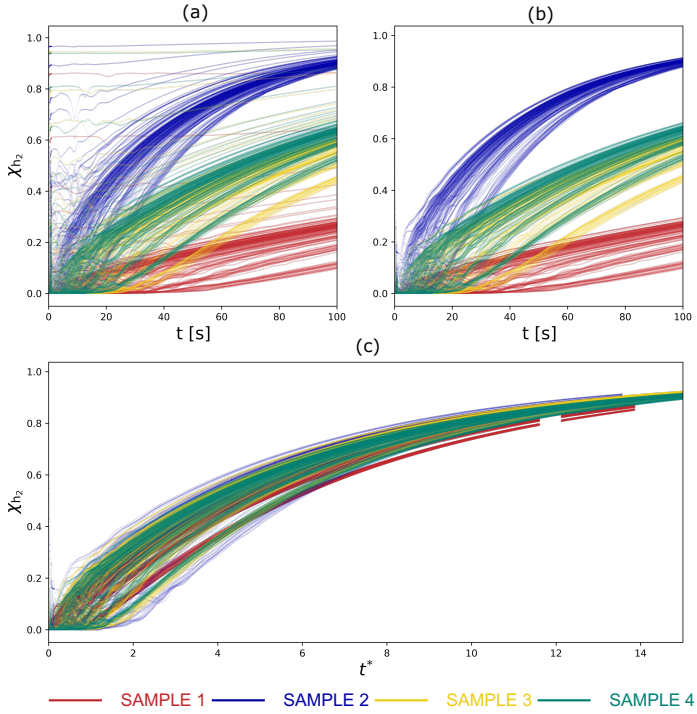

Figure 3. Time series of molar fraction for all four cases. (a) Molar fraction as a function of time for all 152 measurement locations. (b) Molar fraction as a function of time for measurement location satisfying ${r_d}^* > 1/3$. (c) Molar fraction as function of t^* for measurement locations satisfying ${r_d}^* > 1/3$.

Table 3. Values for $\dot{V}/V$ for each case.

Index	$\dot{V}/V$
1	0.002
2	0.019
3	0.006
4	0.007

Fig. 4 shows the evolution of mass fractions as a function of t^*, for a specific value of the non-dimensional height $(2/10)$. It confirms that the two variables in this paper, t^* and ${h_d}^*$, are useful to derive a surrogate model far from the plume (i.e., for ${r_d}^* > 1/3$), where ${r_d}^*$ plays a limited role. In a first step towards a non-dimensional surrogate model, a curve fitting of the data for one specific value of ${h_d}^*$ is performed. To accurately represent the data, the curve should exhibit following features: It should start with an initial molar fraction near 0 and approach 1 as t^* advances; between these values, it should follow an S-shaped pattern, a sigmoid function. As the molar fraction rises rapidly from zero and approaches the asymptote gradually, the lower lobe of the curve should be smaller than the upper lobe. The most basic sigmoid function is the logistic function. A drawback of this function is its symmetrical shape, rendering it unsuitable to fit the dataset. To improve asymmetric accuracy, the five-parameter logistic (5PL) function is used. This function is used in bio-analytics as it provides good fitting for many biological processes [19]. The 5PL function is described by Equation (23).

$$\chi_{h_2}(t^*) = \mathrm{B} + \frac{\mathrm{A}-\mathrm{B}}{\left(1+\left(\frac{t^*}{\mathrm{C}}\right)^{\mathrm{D}}\right)^{\mathrm{E}}}, \tag{23}$$

where A – lower asymptote; B – upper asymptote; C – horizontal location of the transition point; D – slope at the transition point; E – asymmetry of the curve. A 5PL curve is fitted to the data of Fig 4. Two values are predetermined: A is set to 0, and B is set to 1. The three remaining parameters can be consulted in Table 4. To evaluate the statistical quality of the fit, r^2 is calculated and equals 0.997. Thus, statistically the relation in Equation (23) is an accurate non-dimensional surrogate model within the set boundaries. It should be noted that some essential information is lost in this model. Fig. 4 shows that the fit does not accurately represent the data for low values of t^*. As a result, the moment the molar fraction starts rising is not accurately modeled by this curve. Although it is a limited region considering the whole curve, this region is very important for safety purposes as it contains the lower flammable limit of hydrogen at normal temperature and pressure. Other functions presenting a slower rise for low values of t* should be investigated in future works.

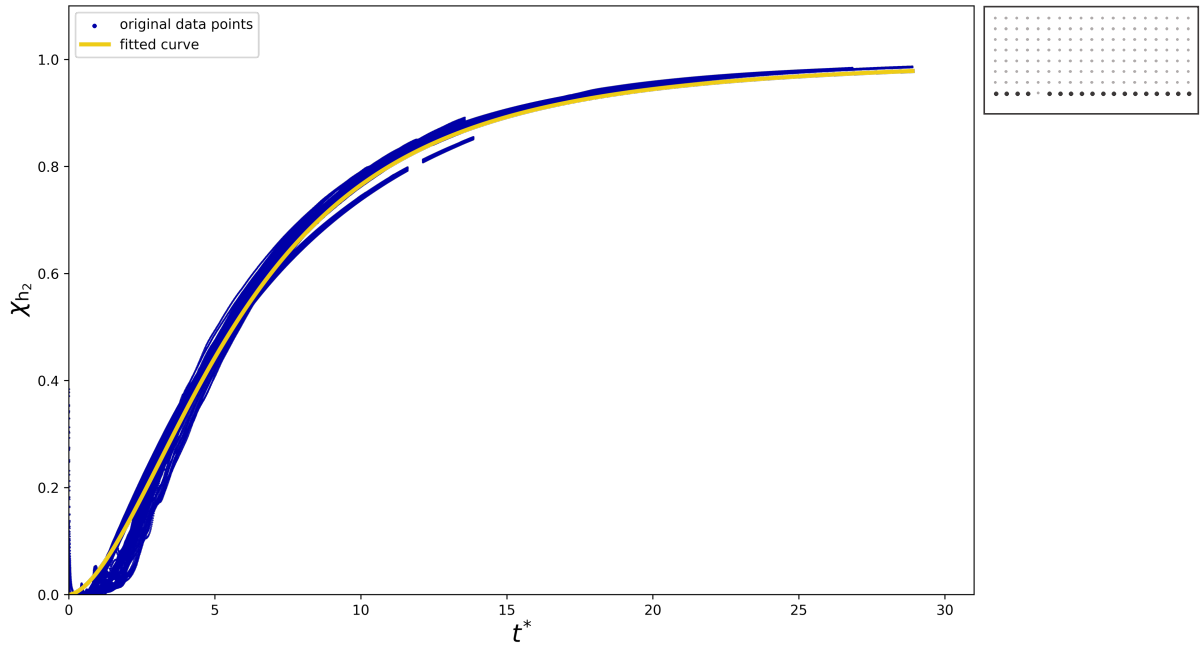

Figure 4. Molar fraction as a function of t^* for ${h_\mathrm{d}}^* = 2/10$.

Fig. 5 shows the evolution of molar fractions as a function of both t^* and ${h_\mathrm{d}}^*$. For different values of ${h_\mathrm{d}}^*$, the characteristic of the best-fit, one-dimensional 5PL curve should vary. However, In the frame of this work, a single 5PL curve was used to fit the whole dataset. The fitted parameters for Equation 23 are shown in Table 4. The resulting value for r^2 is 0.982. The proposed fit is therefore an appropriate non-dimensional surrogate model for the data generated in this paper.

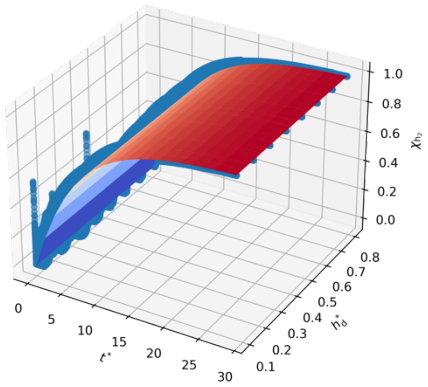

Figure 5. Molar fractions of hydrogen plotted as function of t^* and ${h_\mathrm{d}}^*$. The plot contains two types of data. (1) Measurements at locations satisfying the condition ${r_\mathrm{d}}^* > 1/3$. (2) Contour visualizing the fit based on Equation (23).

Table 4. Fitted parameters of the 5PL function for the one- and two-dimensional fit.

	1D ($h_d{}^* = 0.2$)	2D ($h_d{}^* = 0.2 - 0.9$)
A	0	0
B	1	1
C	8.76	70.7
D	1.69	1.06
E	1.79	13.3

To increase the accuracy of this three dimensional surrogate model, the values of C, D, and E should ideally be functions of $h_d{}^*$. As stated in Section 4, this paper did not include all dimensionless parameters from equation (16). In future works, a multi-dimensional alternative of Equation (23) should therefore be proposed, including all dimensionless parameters from Equation (16):

$$\chi_{h_2}(t^*, h_d{}^*) = B + \frac{A-B}{\left(1+\left(\frac{t^*}{C\left(h_d{}^*, h_0{}^*, \frac{l}{W}, \frac{l}{h}\right)}\right)^{D\left(h_d{}^*, h_0{}^*, \frac{l}{W}, \frac{l}{h}\right)}\right)^{E\left(h_d{}^*, h_0{}^*, \frac{l}{W}, \frac{l}{h}\right)}}, \quad (24)$$

where A – lower asymptote; B – upper asymptote; C – horizontal location of the transition point; D – slope at the transition point; E – asymmetry of the curve. The values for A and B should be 0 and 1 respectively, whereas the values of C, D and E are now function of $h_d{}^*$, $h_0{}^*$, $\frac{l}{W}$ and $\frac{l}{h}$.

6. CONCLUSION

In this paper, the evolution of local concentrations of hydrogen due to stratified filling in a semi-closed space after plume-like releases was investigated, with the purpose of developing a non-dimensional surrogate model to predict this evolution far from the plume as a function of the volume of the geometry and the volumetric flow rate of the release. The proposed surrogate model is derived from results of CFD simulations performed for four different, though similar, dimensional cases. The surrogate model is based on a 5PL sigmoid function and used to predict the evolution of molar fraction of hydrogen as a function of a non-dimensional time and a non-dimensional height. The influence of the non-dimensional distance from the plume $r_d{}^*$ was found to be less relevant and was not considered in this study. The proposed model shows a very good statistical accuracy. Therefore, it can be used to assess the local evolution of hydrogen mass fraction in all similar, dimensional applications. For safety purposes the model's fit should be improved to gain better accuracy near the lower flammability limit of hydrogen. The surrogate should also be extended based on a new set of dimensional cases to account for the whole set of non-dimensional parameters proposed in the analysis. The results show the relevance of dimensional analysis for the study of typical hydrogen leakage cases and the development of adequate surrogate models. In turn, they can be used to cover many dimensional, full-scale applications, and solve optimization problems in an efficient way. They will also ease the use of Uncertainty Quantification for robust optimization.

7. FUTURE WORK

In future works, more sophisticated functions will be tested for both two- and multi-dimensional fits, to further increase the accuracy of the surrogate model, especially at lower values of t^*. Secondly, the model parameters will be further expanded to cover the dimensionless groups proposed in the analysis. To achieve this, a new set of samples will be selected with varying values of all significant dimensionless parameters. Further, Uncertainty Quantification can be used to cover a broader range of cases with slightly varying parameters. Lastly, as this paper only discussed stratified filling far from the plume, the surrogate model will be extended to cover the evolution of molar fraction closer to, and in the plume. To do so, the relevance/impact of $r_d{}^*$ in this dimensional analysis will be thoroughly studied. On the longer term, the results from this paper can be used to train more complex surrogate models. Such a

surrogate model can then be implemented in risk optimization schemes that usually require many time-consuming CFD simulations.

8. ACKNOWLEDGEMENTS

This research is funded by the Belgian Energy Transition Funds (ETF) of the Federal Planning Service for Economy and made possible through the BE-HyFE (Belgian Hydrogen Fundamental Expertise) project.

REFERENCES

1. S. Gupta, J. Brinster, E. Studer, and I. Tkatschenko, "Hydrogen related risks within a private garage: Concentration measurements in a realistic full scale experimental facility," Int J Hydrogen Energy, vol. 34, no. 14, pp. 5902–5911, Jul. 2009, doi: 10.1016/j.ijhydene.2009.03.026.
2. A. Prabhakar, N. Agrawal, V. Raghavan, and S. K. Das, "Experimental investigation on helium distribution and stratification in unventilated vertical cylindrical enclosure – Effect of jet release rates and total release volume," Int J Hydrogen Energy, vol. 41, no. 48, pp. 23213–23228, Dec. 2016, doi: 10.1016/j.ijhydene.2016.10.098.
3. J. M. Lacome, D. Jamois, L. Perrette, and C. H. Proust, "Large-scale hydrogen release in an isothermal confined area," Int J Hydrogen Energy, vol. 36, no. 3, pp. 2302–2312, Feb. 2011, doi: 10.1016/j.ijhydene.2010.10.080.
4. W. M. Pitts, J. C. Yang, M. Blais, and A. Joyce, "Dispersion and burning behavior of hydrogen released in a full-scale residential garage in the presence and absence of conventional automobiles," Int J Hydrogen Energy, vol. 37, no. 22, pp. 17457–17469, Nov. 2012, doi: 10.1016/j.ijhydene.2012.03.074.
5. A. G. Venetsanos et al., "An inter-comparison exercise on the capabilities of CFD models to predict the short and long term distribution and mixing of hydrogen in a garage," Int J Hydrogen Energy, vol. 34, no. 14, pp. 5912–5923, Jul. 2009, doi: 10.1016/j.ijhydene.2009.01.055.
6. K. Prasad, W. M. Pitts, and J. C. Yang, "A numerical study of the release and dispersion of a buoyant gas in partially confined spaces," Int J Hydrogen Energy, vol. 36, no. 8, pp. 5200–5210, Apr. 2011, doi: 10.1016/j.ijhydene.2011.01.118.
7. F. A. C. Viana, C. Gogu, and T. Goel, "Surrogate modeling: tricks that endured the test of time and some recent developments," *Structural and Multidisciplinary Optimization 2021 64:5*, vol. 64, no. 5, pp. 2881–2908, Jul. 2021, doi: 10.1007/S00158-021-03001-2.
8. B. R. Morton, "Forced plumes," J Fluid Mech, vol. 5, no. 1, pp. 151–163, 1959, doi: 10.1017/S002211205900012X.
9. S. Bilyaz and O. A. Ezekoye, "Modeling the dispersion and mixing of light gases in enclosed spaces using the Method of Moments," J Loss Prev Process Ind, vol. 80, Dec. 2022, doi: 10.1016/J.JLP.2022.104877.
10. N. B. Kaye and G. R. Hunt, "Overturning in a filling box," J Fluid Mech, vol. 576, pp. 297–323, 2007, doi: 10.1017/S0022112006004435.
11. G. R. Hunt and N. B. Kaye, "Lazy plumes," J Fluid Mech, vol. 533, pp. 329–338, Jun. 2005, doi: 10.1017/S002211200500457X.
12. W. D. Baines and J. S. Turner, "Turbulent buoyant convection from a source in a confined region," J Fluid Mech, vol. 37, no. 1, pp. 51–80, Jun. 1969, doi: 10.1017/S0022112069000413.
13. R. P. Cleaver, M. R. Marshal, and P. F. Linden, "The build-up of concentration within a single enclosed volume following a release of natural gas," J Hazard Mater, vol. 36, no. 3, pp. 209–226, Mar. 1994, doi: 10.1016/0304-3894(94)85016-X.
14. V. P. Denisenko, I. A. Kirillov, S. Korobtsev, and I. I. Nikolaev, "Hydrogen-Air Explosive Envelope Behaviour in Confined Space at Different Leak Velocities," Sep. 2009, Accessed: Feb. 08, 2023. [Online]. Available: https://www.h2knowledgecentre.com/content/conference423

15. B. Cariteau and I. Tkatschenko, “Experimental study of the concentration build-up regimes in an enclosure without ventilation,” Int J Hydrogen Energy, vol. 37, no. 22, pp. 17400–17408, Nov. 2012, doi: 10.1016/j.ijhydene.2012.03.156.
16. E. Buckingham, “On Physically Similar Systems; Illustrations of the Use of Dimensional Equations,” Physical Review, vol. 4, no. 4, pp. 345–376, Oct. 1914, doi: 10.1103/PhysRev.4.345.
17. I. C. Tolias et al., “Best practice guidelines in numerical simulations and CFD benchmarking f or hydrogen safety applications,” Int J Hydrogen Energy, vol. 44, no. 17, pp. 9050–9062, Apr. 2019, doi: 10.1016/j.ijhydene.2018.06.005.
18. ANSYS Inc., “ANSYS FLUENT 12.0 Theory Guide,” Jan. 2009.
19. “Tech Note: Computing Asymmetric Curves with 5PL and 4PL,” Carlsbad, 2020. Accessed: Mar. 27, 2023. [Online]. Available: www.brendan.com